Case study of solar wind pressure variations and neutral atom emissions observed by IMAGE/LENA.

H. Khan, M.R. Collier and T.E. Moore.

NASA Goddard Space Flight Center, Interplanetary Physics Branch, Greenbelt, MD

Correspondence to:

Hina Khan   Tel: +1 301 286 5947
NASA Goddard Space Flight Center,   Fax: +1 301 286 1433
Interplanetary Physics Branch, Code 692   Email: hina.khan@gsfc.nasa.gov
Greenbelt, MD 20771,
USA.

RUNNING TITLE: Case study of ion outflow with IMAGE/LENA

Abstract

The Low Energy Neutral Atom (*LENA*) imager on the IMAGE spacecraft was designed to observe neutral atom emissions at low energy (10 eV - ~4 keV) from the high-latitude ionosphere. In this study we present data from an ion outflow event on June 24, 2000 showing increases in neutral flux that appear to be associated with dynamic pressure variations in the solar wind. Results from a correlation analysis show the neutral flux to be well correlated (~0.64) with the solar wind dynamic pressure. The neutral atom data are most consistent with a source region at a radial distance of 2.2-2.3R_E, interpreted as the region over which the bulk ion outflow escapes the ionosphere and is partly converted to neutral atoms. Very short time delays (~2 min) were calculated between the solar wind pressure increase and neutral atom response, indicating a prompt ionospheric response to the solar wind input.

1. Introduction

The terrestrial ionosphere supplies a substantial amount of plasma to the magnetosphere during intense geomagnetic activity, such as during a magnetic storm event (e.g. Shelley *et al.*, 1972). The mechanisms by which ionospheric ions enter the magnetosphere and the influence they have on the dynamics of the system are still not fully understood. Statistical studies in the high-latitude magnetosphere during high magnetic activity have shown variable ionospheric O^+ fluxes in the plasma sheet, ring current (Lundin *et al.*, 1980; Lennartsson, 1992), and the tail lobes (Sharp *et al.*, 1981). In-situ satellite observations have been made of keV upflowing ions along auroral field lines (Shelley *et al.*, 1976), and originating from the auroral ionosphere (Collin *et al.*, 1998). Over the last few years, it has become clear that the dayside merging region, the cusp, is a significant source of upflowing ions (Yau *et al.*, 1985; Waite *et al.*, 1985; Moore *et al.*, 1986; 1990; Pollock *et al.*, 1990). Further studies have demonstrated the variation of the outflow events with solar cycle, season and magnetospheric activity (Yau and Lockwood, 1988; Øieroset *et al.*, 1999).

Correlation analyses have been performed to better understand the relationship between the solar wind and geomagnetic variables and the outflow events (e.g. Giles *et al.*, 1993, Moore *et al.*, 1999). Pollock *et al.* (1990) demonstrated a strong correlation between IMF B_z and the invariant latitude of the peak upwelling O^+ flux. More recently, Øieroest *et al.* (1999) concluded that the intensity of outflow in the cusp region and the postnoon sector undergoes some increase during southward IMF conditions, but that the outflow depends more strongly on *AE*. They also categorised the outflow events observed by the Viking satellite into ion conics, beams and hybrids. Their results indicated that in the cusp region the outflow events are dominated by ion conics, whilst in the prenoon and postnoon sectors ion beams accounted for the majority of the outflow events.

It has been suggested that the ion acceleration processes responsible for the ion outflow are altitude dependent (e.g. André and Yau, 1997). Energetic precipitating electrons deposit energy at low altitudes below the *F*-region peak (~120-200 km), as does 'joule' or frictional heating. Since the plasma is collision dominated at these altitudes, low altitude heating processes have little effect on the topside ionosphere initially and can take around 20 min or more to influence the topside *F*-region (e.g. Heelis *et al.*, 1993). However, low energy electrons deposit a large amount of energy into ionospheric electrons at or near the exobase (~350-1000 km), causing an increase in the ionospheric scale heights and accelerating light ion outflow (Horwitz and Moore, 1997). The scale height increase near the exobase results in the rapid escape of ions from the ionosphere. As 1-2 eV O^+ ions move to altitudes >1000 km, they undergo transverse (to the magnetic field) heating to energies ~10eV; ions of energies greater than this will escape the terrestrial gravitational field. The bulk of escaping ionospheric O^+ is found in this transitional energy (Moore *et al.*, 1986). At altitudes of several thousand kilometres there is an O^+ population with total flux 10^8-10^9 cm^{-2} s^{-1} (Pollock *et al.* 1990) and perpendicular temperature of ~10eV (Moore *et al.*, 1986). At higher altitudes, the ions are accelerated further, but the charge-exchange probability rapidly decreases with altitude due to parallel acceleration by $E_{||}$ and centrifugal effects.

Identifying which heating processes are responsible for the upwelling ions requires observations and studies on timescales < 20min. All the studies mentioned thus far used in-situ satellites, so that only the long term variability of the ion outflow events could be addressed (e.g. Yau *et al.*, 1985). Observations on shorter timescales have not been possible because observing the 'global' nature of ion outflow with respect to local time from the Earth requires several months of data to allow the satellites to precess in their orbit in local time.

Thus it has been very difficult to understand the evolution of ion outflow in local time and investigate the initial acceleration mechanism. These problems were addressed by the launch of the IMAGE spacecraft (Burch *et al.*, 2000), which includes a low-energy neutral atom (*LENA*) imager to observe neutral ions escaping the ionosphere via auroral processes in the energy band ~10 eV-1 keV (Ghielmetti *et al.*, 1994; Moore *et al.*, 2000). Some of the outflow events observed by *LENA* appear to be directly driven by solar wind dynamic pressure, in some cases dramatic neutral flux increases are associated with the arrival of a coronal mass ejection (Moore *et al.*, 2001; Fuselier *et al.*, 2001). The 2 min cadence of IMAGE has helped determine that ion outflow events can respond very rapidly (a few minutes) to enhancements in the solar wind.

Fuselier *et al.* (2002) studied an event where dynamic pressure enhancements appeared to be a direct driver for increases in outflow fluxes. They further suggested, upon visual analysis of the data, the acceleration mechanism responsible for the outflow reacted within a few minutes of the arrival of the solar wind disturbance. In this paper we perform a complementary study of the event examined by Fuselier *et al.* (2002), including a detailed correlation analysis. *LENA* has the ability to break the neutral atom outflow into mass species, and we show the relationship of each ionospheric outflow species, H and O, to the dynamic pressure variations. We have taken into account the divergence of neutral atom flux from a localised source and thereby derived information about the spatial distribution of the source as well as its temporal dynamics. Section 2 describes the instrumentation used in this study. Section 3 gives the specific observations used, and section 4 describes our analysis. Sections 5 and 6 summarise our results and conclusions.

2. Instrumentation

The Low Energy Neutral Atom (*LENA*) imager on IMAGE is one of three neutral atom imagers on the spacecraft and has the unique capability of observing energetic neutral atom emissions in the low energy range of 10 eV to ~1 keV (Moore *et al.*, 2000). The detection process uses a new atom-to-ion surface conversion technology to convert a fraction of the incoming energetic neutral atoms to negatively charged ions that can then be detected using standard electrostatic optics and time-of-flight techniques. From this the mass, energy and arrival direction of the neutral atoms in azimuth and polar angle can be determined (Wurz *et al.*, 1995). The energy range of *LENA* allows the detector to not only image energetic neutral atom emissions resulting from escaping ions accelerated via auroral processes, but also directly observe more energetic populations such as the ring current and the solar wind neutral atoms, which are mainly neutral hydrogen (Collier *et al.*, 2001). Energetic incident solar wind neutral atoms can cause 'sputtering' of negative ions from the conversion surface. This process allows *LENA* to observe neutral atoms to energies of ~4 keV. In general, the sputtering of oxygen off the conversion surface atoms occurs when the energy of incident hydrogen exceeds a few 100 eV, whilst energetic neutral O can readily sputter H^- and O^- from the conversion surface at all energies (Moore *et al.*, 2000). Thus the incoming energetic neutral atom signature detected at *LENA* is a combination of the actual neutral atom outflow from a particular source or event and any sputtered ions off the conversion surface. The sputtered ions have significantly less energy than the incident ions, with their angular dispersion clearly broader than the incident signal of converted ions. Also other analysis techniques can be used to distinguish between these two factors. This issue will be addressed further in the analysis.

The *LENA* imager also consists of a collimator and charged particle rejector, which depending on the voltage setting can reject particles with energy/charge <100 keV/e. The *LENA* field-of-view spans ±45° from the direction radially outward. There are 45 azimuthal sectors each of which sweeps out 8° as the spacecraft spins providing a total image of 90° x 360° in 12 x 45 pixels of 8° x 8°, through an aperture of ~1 cm^2. The spacecraft roll is in a reverse cartwheel mode and completes one spin in ~2 min. At launch in March 2000, IMAGE had an apogee of ~8 R_E geocentric in the northern hemisphere and perigee of ~1000 km altitude, with an inclination of 90°.

3. Observations

Data from the *LENA* imager on IMAGE will be presented for June 24th, 2000 between 0100-0300 UT. IMAGE was increasing in altitude during this interval with the perigee pass recorded at 0045 UT. It has been suggested that the optimal location to observe outflow is in the polar region close to the Earth (within ~4R_E) as this location maximizes the outflow signal against the minimum in background from charged particles (Fuselier *et al.*, 2002). Figure 1 shows orbit of the IMAGE in the GSM *X-Z* plane and the *X-Y* plane during the interval of interest. At 0100 UT, IMAGE was located very close to the equatorial plane on the dusk side of the Earth. The spacecraft then increased in altitude towards apogee, travelling over the polar cap providing a good view of the high-latitude ionosphere to observe potential outflow events.

3.1 Solar wind conditions

On June 24th, 2000, Geotail was located just upstream of the bow shock very close to the subsolar region, with GSM $(X,Y,Z) \approx$ (+18.0,+1.0,-2.6) R_E at 0100 UT, and so serves as a

reliable upstream monitor (Collier *et al*., 1998). Upstream conditions were obtained using the Comprehensive Plasma Instrument (Frank *et al.*, 1994) and the Magnetic Field Experiment (Kokubun *et al.*, 1994) at a resolution of ~45 sec and 3 sec, respectively. All magnetic field and spacecraft position data presented in this paper are in GSM coordinates. Figure 2 shows the observations obtained from Geotail during the 2hr interval 0100 UT-0300 UT. The seven-panel plot shows the interplanetary magnetic field components, B_x, B_y, B_z and total field B_T, followed by the solar wind density, velocity and pressure.

The magnetic field in B_Z and B_y were predominately northward and dawnward during the 2hr interval with a slight southward shift in B_Z just after 0100 UT. The solar wind density was substantially higher than average from ~0115 UT to ~0220 UT. The solar wind velocity decreased from ~580 km s^{-1} to 540 km s^{-1} at the onset of the first density intensification (10 to 20 cm^{-3}) at 0115 UT, and then increased only slightly to 560 km s^{-1} during the further density enhancements (~45 min). This suggests that the density bursts were related to pressure pulses impacting the magnetopause as opposed to a response from an interplanetary shock. This is confirmed in the last panel in Fig. 2 where three distinct pressure increases were observed by Geotail at ~0115 UT, ~0133 UT and ~0145 UT. It is interesting to note that at the peak of the last of these three events, the total field dropped to only a few nT, but then recovered quickly thereafter. Also this last event was much more prolonged than the others and there appeared to be an indication of a fourth density increase at ~0205 UT. This occurred at the time of an increase in the solar wind velocity, but then decreased rapidly for the remainder of the interval. The field remained steady after this event, and the density returned to close to values at the start of the interval.

3.2 LENA observations

Plate 1 shows the start, stop and coincidence spectrograms of the *LENA* observations from 0100-0300 UT. The vertical axis in each panel gives the spin angle information relative to the Earth. The top two panels show the 'start' and 'stop' data with the colour-coding representing the count rate of the neutral population. The bottom panel shows the coincidence data for all events recorded, scaled into flux units. This then illustrates the actual outflow data recorded by the instrument, and converts the intensity into flux. The thin white lines in each of the panels represent the direction and angular extent of the Earth. The diffuse emission 'band' between 90° and 180° is a signal believed to be the neutral atom emission from the magnetosheath, the 'sun pulse' (Collier *et al.*, 2001).

At the start of the interval, a high level of background was observed as the spacecraft travelled through the radiation belts and very close to the Earth. IMAGE passed perigee at 0045 UT, and the observations here are from the outbound flight. Close to the Earth, the imagers are very sensitive to high-energy particles and as a result cannot image ionospheric outflow. Once through the radiation belts and the perigee pass, the flux rates return to normal level. The background level dropped to a minimal rate and the diffuse sun pulse appeared just after 0120 UT. After 0120 UT clear bursts of intense outflow events were observed by *LENA* at ~0125 UT, ~0135 UT and ~0150 UT. These were identified by the intense flux increase in a localised region close to the limbs of the Earth. The events were observed in both the 'start' and the 'stop' data indicating that these events were very intense features. This was confirmed in the event data panel where peak fluxes of ~10^6 cm^{-2}s^{-1} were observed, which is typical for outflow events (e.g. Yau *et al.*, 1983). Notice that at the beginning of the outflow bursts (~0120 UT) the peak flux was observed slightly off the limb of the Earth. As the events progressed, the peak flux appeared to move over the polar cap towards the other side of the Earth. The most likely scenario is for the outflow to be accelerated from auroral

regions and then charge exchange at high altitudes to produce the energetic neutral atom emissions observed by *LENA*. A smaller event was perhaps recorded at ~0200 UT.

One important feature to point out in this data set is the apparent increase in the overall flux rate just after ~0120 UT. When the spacecraft travels close to the Earth and through the radiation belts, the bias voltages on the micro-channel plates are lowered to protect the detectors on the instrument. Upon completion of the pass the bias voltages are returned to normal operating levels. On close inspection of the state log (not shown here), where all commanding details are documented, this change in bias voltages occurred at 0120 UT. This change came into effect within sub-spin timescales, marking the return to normal operating levels. Therefore to remain consistent in this analysis, only observations made following the return of the channel plate bias voltages to the normal operating level (post 0120 UT) are considered. The data recorded in the next spin cycle will have implemented the change in the bias voltages and record the data accordingly.

Figure 3 shows IMF B_z and solar wind pressure in the top two panels, followed by the SYM-H index, which is used as a proxy for Dst. The lower three panels present the raw background corrected mass separated *LENA* data (H, O and total counts, respectively) summed over an azimuth range (–90° to +45°) with the Earth at 0°, to concentrate on those emissions associated with the outflow. The count rates have not been modified to include the efficiency of the instrument response. Only the raw counts separated by time-of-flight for the different mass species have been plotted. The effect of the solar wind pressure enhancements on the outflow is obvious, with a clear response in neutral H and O resulting from charge exchanged H^+ and O^+ outflow. There appears to be a direct relationship between the solar wind pressure and the neutral atom emissions of outflow. However, there remains an ambiguity in the

timing of the events, stemming in part from the uncertainties in accurately calculating the delay between features observed at Geotail and the impact at the magnetopause, and a delay between the initiation of the outflow events in the ionosphere and observations at IMAGE. To try to resolve any other timing issues, we present a cross correlation analysis of each mass species of the outflow and the solar wind dynamic pressure. Also, Figure 3 suggests that the raw neutral O count rate dominates over the neutral H count rate signature by a factor of two, however the instrument response has not been included in the dataset.

4. Discussion

4.1 Cross Correlation Analysis

For the correlation analysis, the *LENA* data were first background corrected to remove any systematic effect that may be present associated with the ambient background noise level. Further the data were separated into their constituent mass species from the time-of-flight information, and were averaged over the azimuthal range $-90°$ to $+45°$ relative to the Earth direction so that only those data associated with the outflow emissions were included in the cross correlation. From Plate 1, one can see that this azimuthal range encompassed the bursts of neutral atom emissions. The two species, H and O, were then used in separate cross correlation analyses. Cross correlation coefficients of neutral H and neutral O from 0120 UT (i.e. after the change in the bias voltages) to 0230 UT with solar wind dynamic pressure were calculated versus time lag over an interval of ±60 min, with a resolution of 2 min (the spin resolution of IMAGE). For positive lags the solar wind dynamic pressure leads the ionosphere, while for negative lags the ionosphere (unphysical) leads the solar wind.

Figure 4a and 4b present the cross correlation results of the neutral H and O, respectively, with dynamic pressure over a time lag of ±60 min. The top graphs show the raw data used in the cross correlations, with the solid line profiling the solar wind data and the dashed line tracing the background corrected neutral H and O count rate from 0120 UT to 0230 UT. The solar wind data were plotted over the longer time interval of 0020 UT to 0330 UT, to illustrate the data used in the cross correlation algorithm over the lagged time of ±60 min. The lower graphs show the cross correlation coefficients versus time lag. The error bars show the standard error of the coefficient, given by $\varepsilon = (1-r^2)/(n-2)^{1/2}$, where r is the value of the cross-correlation coefficient and n is the number of data values from which it was determined. The dot-dash lines show the 99% significance level derived from Student's t-test; cross-correlation coefficients with magnitudes smaller than this are not considered statistically significant.

The top graph in Figure 4a clearly show the three peaks in the dynamic pressure data at the times mentioned (solid line). Correspondingly, there are enhancements in the neutral H signal (dotted-dashed line) which appear to occur promptly after the pressure increases. However, the cross correlation coefficients (lower graph) do not reveal any significant peak for positive (physical) lags to suggest that there was a clear relationship between these parameters. A statistically significant peak correlation of 0.68 was calculated at an unphysical lag of -12 min, with a secondary peak of 0.38 at 2 min time lag. Unfortunately this secondary peak was just below the significance threshold level set by the Student's *t*-test.

Moving onto Figure 4b, the top graph shows the neutral O signature overlaid on the solar wind dynamic pressure data, as in Figure 4a. There were three clear intensifications in the neutral O observations, which again promptly followed the pressure pulses. However, yet again, when the cross correlation analysis was performed the results were inconclusive. In the

lower graph, the overall trend in the cross correlation curve was very similar to that presented in Figure 4a. A peak correlation coefficient of 0.71 occurred at -14 min, which again is unphysical in magnetospheric terms. There was a secondary peak at 2 min lag, with a correlation value of 0.31, however this was again well below the 99% significant level and cannot be used in the analysis to represent a statistically significant data peak.

4.2 Problems with the cross correlation

We have taken the datasets as outlined above and performed a cross correlation analysis to try to determine the relationship between these parameters and establish the timing delay between the events. Although there appears visually to be a correspondence between the solar wind dynamic pressure and the raw neutral density, quantitatively we were unable to establish a physically meaningful and statistically relevant correlation between these parameters.

One factor that needs to be taken into account is the divergence of flux observed by *LENA* away from the region emitting the energetic neutral atoms. IMAGE views the Earth from a wide range of altitudes, whereas the majority of the neutral atom emissions extend from a localised region in the auroral zone (e.g. Moore *et al.*, 1985; Shelley, 1985; Fuselier *et al.*, 2002). Previous studies have shown that the upwelling ion flux signatures maximise near the low-latitude edge of the outflow event and may be regarded as the source region of the outflow (Lockwood *et al.*, 1985; Pollock *et al.*, 1990). This region is characterised by those ions that display the shortest flight paths from source to observer and those with the largest field-aligned velocities, with slower particles convecting further poleward of the spacecraft. As IMAGE increases in altitude, the observed neutral particle flux from a point source will fall off as $1/r^2$, where r is the radial distance to the spacecraft. If the bulk of the escaping ionospheric ions were accelerated from a particular source region

then the neutral particle flux associated with the escaping ions will also vary with $1/r^2$ and *LENA* would only observe a fraction of the actual neutral atoms produced through charge exchange with these ionospheric ions. Therefore, to accurately establish the intensity of the outflow, one must scale the *LENA* observation with respect to the radial distance to the source region, *h*, the radial distance at which the acceleration processes maximise the bulk of the escaping neutral flux. The scaled outflow would then represent the total neutral flux escaping the source region with no degradation of the signal due to distance of the observations from the source.

4.3 Modification to the cross correlation analysis

To determine the radial distance to the source region of the ion outflow the data were scaled by a factor $1/(r-h)^2$, where *h* represents the source distance, and *r* is the radial distance to the spacecraft at the time of the observations (assuming the emissions occur along the Earth-IMAGE line). The square law variation of this parameter was used as an initial estimation. Further analysis showed (not shown here) that the variation of the exponent between 1.75-2.25 to investigate the suggestion of an extended source region did not alter the overall results for determining the source distance. Thus for the remainder of the analysis an exponent of 2 was implemented.

The spacecraft moved a distance of $\sim 4\,R_E$ during the course of the data interval. Therefore only the most energetic ions associated with the outflow will charge exchange into neutrals observable at *LENA*; most likely only a fraction of the actual outflow observable at lower altitudes. The data were then normalised to the altitude of the peak outflow event observed, at $3.52\,R_E$. For initial analysis purposes, a source region radial distance of $1.5\,R_E$ was used, which is a typical source region distance for ion outflow events in the energy band observed

(e.g. Moore *et al.*, 1986; Pollock *et al.*, 1990). It could be possible that the source region was located close to the spacecraft; further from the Earth. However the exospheric density falls off as $1/r^3$, which is the same as the drop off rate of ion flux with distance from the source region. Therefore for the same amount of ion flux produced from the source region, there will be a higher rate of neutral flux production by charge exchange close to the Earth where the exospheric density is higher. Further away, the exospheric density is much lower leading to less charge exchange interactions to produce the neutral flux. Considerably more ion flux would be required to produce a significant neutral signature at higher altitudes where the exospheric density is lower. Thus it is more likely that the source region was located close to the Earth, as we would expect to be able to observe the charge exchanged neutral flux population much more readily.

The results of the cross correlations from this modified data set are shown in Figures 5a and 5b, in the same format as Figures 4a and 4b. The top graph in Figure 5a presents a time series of the neutral H counts and the solar wind dynamic pressure data. The three enhancements in both data sets are very clear and the neutral atom data were scaled to account for the increase in radial distance of the spacecraft from the source region. Since the intensity falls off at the rate described above, in order to compensate for this effect the neutral atom data were scaled to give the intensity of the outflow at the source region distance. Thus the scaling factor was largest when the IMAGE was the furthest from the source. The cross correlation coefficients shown in the middle graph plotted versus time lag display a very distinct peak of 0.64 at 2 min time lag well above the significance threshold. The bottom graph shows the scatter plot of the neutral H and solar wind pressure data plotted at the time of the peak correlation coefficient. The solid line indicates the linear least-square fit to the data. There is an obvious trend in the data resulting in the cross correlation results shown. Figure 5b shows the

corresponding results from the neutral O emissions. Again the top graph plots the count rate and pressure data in a time series that were used in the correlation. The cross correlation coefficients produce a slightly lower peak of 0.60 but at a consistent lag of 2 min between the data sets.

A positive time lag between the data sets indicates that the ionospheric outflow occurred after the pressure variations were observed at Geotail. It should be noted that no propagation delay has been taken into account at this stage. Geotail was located ~18 R_E upstream with the solar wind velocity observed to be ~540 km s^{-1}. By carefully studying the IMF field parameters, it was possible to estimate the orientation of a phase front carrying the field and plasma discontinuities in the solar wind, and hence estimate when the solar wind features were likely to impact the magnetosphere. The orientation of the planar phase front was determined at the start of the pressure enhancements at 0115 UT, where there was also a change in the magnetic field direction. It was found that the phase front carrying the discontinuity with the change in the field direction was substantially tilted out of the ecliptic plane, thus allowing the solar wind pressure variations to impact the magnetosphere sooner than may be expected. Using typical propagation delay algorithms (e.g. Khan and Cowley, 1999), the time delay between Geotail and the subsolar magnetopause assuming a perpendicular phase front was 7 min. However, since the discontinuity was substantially tilted in this instance, this delay would be significantly reduced. Thus at the time the solar wind features were observed at Geotail, part of the discontinuity phase front was much closer to the magnetosphere than the GSM *X* position of the spacecraft, most likely inside the magnetosheath. This would then account for the prompt arrival of the phase front and produce an outflow response which was not significantly delayed from the *LENA* observations. Furthermore, there will a 1-2 min error associated with any time shift due to the approximate representation of the phase front.

It is clear from the data that the outflow observed at *LENA* responded very quickly to the arrival of the pressure variations in the ionosphere. This suggests that the dominant species of the outflow is most likely to be neutral hydrogen. However, Fig. 3 and Fig. 5b indicate that the raw oxygen count rate was a factor of two higher than the raw neutral H signature. This was due to the sputtering of oxygen off the conversion surface. As discussed earlier, energetic neutral hydrogen readily sputters oxygen neutrals off the conversion surface of the detector. Since the time delay between the observed neutral atom signatures and the pressure variations was very short (relative to the resolution of the data), it was likely that the dominant outflow species was hydrogen, and the oxygen signal was a result of sputtering from the most energetic hydrogen neutrals. Oxygen neutrals propagate four times slower than hydrogen neutrals of the same energy. Therefore there would be a significant delay between the pressure variations and the arrival of an oxygen signal from the source. Since this was not the case, one can assume that the oxygen signal detected was a result of sputtering from energetic hydrogen and not outflow from the source.

In the data presented in Figures 5, an arbitrary radial distance to the source region of 1.5 R_E was used to scale the data as observed at the spacecraft. The cross correlation algorithm can be used to provide a better understanding of the source region by repeating the analysis with a variable radial distance to the source region of up to 3 R_E. The maximum in the peak cross correlation coefficients as a function of source region radial distance can then be interpreted as the distance of the outflow acceleration region. The cross correlation peak coefficients were determined as a function of the assumed source region distance, with the results for each mass species plotted in Figure 6. The neutral H source region distance curve (solid line) exhibits a shallow curve, with a steady increase to a radial distance of ~2.2 R_E, before falling

off rapidly after this. The vertical solid line indicates the peak was located at a radial distance of 2.18 R_E. Moving onto the dashed curve which displays the neutral O cross correlation coefficients, we notice that these data increase more steeply at lower radial distances reaching a peak ~2.3 R_E (dashed vertical line) and then decreasing rapidly thereafter. The peak in each of these curves can then be considered the most likely radial distance to the source region; the region at which the bulk ion outflow escapes the ionosphere resulting in the interaction with the neutral atoms observed by *LENA*. For each species a source region of 2.2-2.3 R_E was calculated from the centre of the Earth. This is consistent with previous studies of distance to the source region for escaping ion flux in the energy range observed here.

Fig. 7a and 7b show the corresponding cross correlation curves and scatter plots, in the same format as the previous figures. Each species has been plotted with the relevant source region distance calculated from Figure 6. It is clear from Figs. 7 that these data are much better correlated than when an arbitrary source region distance was used. Peak cross correlation coefficients of 0.67 for H and 0.66 for O at a consistent 2 min lag were obtained.

5. Summary

In this study we have presented data from 24th June 2000, where there appeared to be a clear relationship between solar wind dynamic pressure variations observed by Geotail, situated upstream of the bow shock, and bursts of energetic neutral atom emissions observed by *LENA*. IMAGE was passing close to the Earth just prior to the events and then increased in altitude during the course of the observations. This placed IMAGE in prime position to observe these outflow events. We presented a cross correlation analysis of the *LENA*

emissions and the solar wind pressure data which establishes the relationship between these parameters, the promptness of the outflow, and the radial distance to the source region.

Upon initiating the study, it became clear that the relationship between the solar wind dynamic pressure and the neutral hydrogen and oxygen signatures were not entirely straightforward. Figures 4a and 4b show the cross correlation results obtained using the background corrected counts from *LENA* separated into mass species and the dynamic pressure data. The results of this analysis suggested that other factors were involved in any relationship between the dynamic pressure and *LENA* fluxes seen at IMAGE. This led to further investigation of the data to try to understand why the results were not as obvious as were initially thought. The details of the factors considered in the analysis were outlined and addressed in the later paragraphs in Section 4.

The principal factor in the re-analysis of the data was the effect of the increasing altitude of the spacecraft on the flux of neutral atoms at the IMAGE spacecraft during the period of enhanced solar wind pressure. Assuming a narrow auroral zone source for the low energy neutral atom fluxes, which would be unresolved by the imager, the flux of neutral atoms at the instrument aperture falls off as $1/r^2$, where r is the radial distance from the site of the charge exchange producing the energetic neutral atoms. Only those outflow ions with sufficient energy to charge exchange at high altitudes would produce a detectable signal at *LENA*. Prompt energetic neutrals observed at the spacecraft would have been formed by charge exchange from relatively energetic source ions, and the greatest ion energization in auroral acceleration region occurs at ~2R_E. This region is defined as the region where the bulk of the ionospheric ions attain sufficient energy to escape the terrestrial field producing charge exchanged neutrals at higher altitudes. However, since the actual source region distance was

not known a priori, we allowed the radial distance to the source region, *h*, to be a free parameter, such that the source flux was assumed to diverge as $1/(r-h)^2$ from that source region. Although a point source was assumed in the final analysis, the exponent of the scaling factor was varied and it was found that the eventual result of the distance to the source region did not change when exponents between 1.75 and 2.25 were used. Therefore a square law dependence was deemed sufficient for the purposes of this study.

With this additional factor and generalised source region assumption, the cross correlation analysis was revisited. The results were much more promising, revealing a statistically significant and physically realistic peak in the cross correlation coefficients for both the neutral H and O emissions. The delay time from the analysis revealed a 2 min delay within the errors of the propagation parameters discussed earlier, implying that the ionospheric response was extremely prompt after the impact of the pressure pulses on the magnetosphere. Upon investigating the solar wind and IMF data further, we were able to estimate the orientation of the phase front carrying the solar wind and IMF discontinuities towards the magnetosphere. The phase front orientation was found to be highly titled out of the ecliptic plane suggesting that the pressure enhancement might impact the magnetosphere around the same time as the data were recorded at the spacecraft. This would account for the prompt response in the outflow data to the impact of pressure variations at the magnetopause. Also there will be at least a 1-2 min error in the propagation delays due to the estimation of the orientation of the phase front, and an error of the order of the 2 min spin cycle in the travel time of the outflow neutral atom signal from the source region to *LENA*.

Finally, by varying the radial distance to the source region in the scaling of the *LENA* data, we were able to perform systematic cross correlations over a range of source height radial

distances to gain an understanding of where the source region of the outflow ions for these events was located. Figure 6 showed that the peak in the cross correlation coefficients increased with the radial distance to the source region to a maximum value before falling off with increasing distance. The source distance curve indicated the most likely radial distance where the accelerated ionospheric ions were converted to neutrals escaping the geomagnetic field. A radial distance of ~2.2-2.3 R_E was calculated for the source region, which is consistent with previous suggestions for this interaction region (e.g. Yau and André, 1997). The cross correlograms for each species were re-evaluated with the calculated distance to the source region information. The correlation curves were more defined and revealed higher absolute peak values at a consistent time lag of 2 min.

6. Conclusions

Based on our correlation analysis of solar wind and terrestrial energetic neutral emissions, we conclude that the enhanced dusk sector energetic neutral atom emissions were indeed temporally associated with solar wind dynamic pressure fluctuations in this event. Significant correlations were observed to a confidence level of over 99% when the neutral atom emissions were assumed to radiate from a small source region located at a radial distance of 2.2-2.3 R_E, with a time delay of ~2 min from the solar wind pressure profile. We conclude that the ion outflows producing these neutral atom emissions were dominated by protons of the type that are aurorally accelerated to greater than 1 keV energy in the region of low plasma densities above the active auroral displays. The oxygen atoms were likely to be produced from sputtering effects rather than a source from the outflow region. This conclusion was based on the rapid response of both species, which for oxygen can only be accounted for through sputtering effects.

Figure Captions

Figure 1.   Projection of the IMAGE orbit in GSM *X-Z* plane (top) and GSM *X-Y* plane (bottom). The orbit is shown for 0100-0300 UT on the 24th June 2000.

Figure 2.   Solar wind and IMF data obtained by the Geotail spacecraft for the interval 0100-0300 UT. From top to bottom the panels of the figure show the three GSM components of the IMF together with the field strength, and the density, velocity, and dynamic pressure of the solar wind.

Plate 1. *LENA* time-of-flight spectrogram plotted in spin angle versus time; 0100-0300 UT on the 24th June 2000. The data are colour-coded to indicate the intensity of the emissions. The top two panels show the 'start' and 'stop' singles rates, whilst the bottom panel shows the coincidences, time of flight event displayed in flux units. The white lines indicate the direction and extent of the Earth. The diffuse band between 90° and 180° is ENA emission from the magnetosheath.

Figure 3. A time series combining the solar wind data and the LENA observation averaged over an azimuthal range centred about the Earth. The IMF B_Z GSM data are shown at the top, followed by the solar wind dynamic pressure, the SYM-H index which is a proxy for Dst, and the mass separated background corrected *LENA* data, H, O and total counts respectively.

Figure 4.   Results of the cross correlation analysis between solar wind dynamic pressure and the (a) neutral Hydrogen and (b) neutral Oxygen for the time interval 0120 UT-0230 UT. The upper panels shows the data used for the cross correlation analysis. The solid line shows the

solar wind dynamic pressure data from 0020-0330 UT, whereas the dot-dashed line shows the (a) neutral hydrogen and (b) neutral oxygen 0120-0230 UT. The lower panel shows the value of the cross-correlation coefficient versus lag in the interval ±60 min at 2 min resolution, with positive lags representing the physical scenario in which the solar wind leads the ionospheric outflow. The zero lag represents the cross correlation at the time of the *LENA* observations. The horizontal dot-dashed lines show the 99% significance level calculated by the Student's *t*-test.

Figure 5. As for Figure 4 but now with the LENA data scaled by a factor of *$1/(r-1.5R_E)^2$* to account for the spacecraft distance from an assumed source height of 1.5 R_E. The vertical dot-dashed line marks the peak in the cross-correlogram. The lower panels provide a corresponding scatter plot of the solar wind dynamic pressure versus neutral atom species, plotted at the lag of the peak correlation coefficient shown in the plot above. The solid line shows a linear least-squares fit of the pressure to the neutral atom species.

Figure 6. Radial distance to the source region versus peak in the cross correlation coefficients for each neutral atom species over the time interval 0120-0230 UT. The solid line shows the peak correlation coefficient from neutral Hydrogen varying with source height, whilst the dashed line indicates the neutral Oxygen variation. The vertical lines indicate the maximum in each curve.

Figure 7. As for Figure 5 but now with the *LENA* data scaled by a factor of *$1/(r-h)^2$* where *h* is 2.18 R_E for H (a) and 2.30 R_E for O (b).

References

André, M and A.W. Yau, Theories and observations of ion energization and outflow in the high latitude magnetosphere, *Space Sci. Rev.*, *80*, 27, 1997.

Burch., J.L., IMAGE mission overview, *Space Sci. Rev.*, *91*, 1, 2000.

Collier, MR., J.A. Slavin, R.P. Lepping, A. Szabo, and K. Ogilvie, Timing accuracy for simple planar propagation of magnetic structures in the solar wind, *Geophys. Res. Lett.*, *14*, 2509, 1998.

Collier, M.R., et al., Observations of the neutral solar wind, *J. Geophys. Res.*, *106*, 24893, 2001.

Collin, H.L, W.K. Peterson, O.W. Lennartsson, and J.F. Drake, The seasonal variation of auroral ion beams, *Geophys. Res. Lett.*, *25*, 4071, 1998.

Frank, L.A., K.L. Ackerson, W.K. Peterson, J.A. Lee, M.R. English, and G.L. Pickett, The comprehensive plasma instrumentation (CPI) for the GEOTAIL spacecraft, *J. Geomagn. Geoelectr.*, *46*, 23, 1994.

Fuselier, S.A., A.G. Ghielmetti, T.E. Moore, M.R. Collier, J.M. Quinn, G.R. Wilson, P. Wurz, S.B. Mende, H.U. Frey, C. Jamar, J.-C. Gerard, and J.L. Burch, Ion outflow observed by IMAGE: Implications for source regions and heating mechanisms, *Geophys. Res. Lett.*, *28*, 1163, 2001.

Fuselier, S.A., H.L. Collin, A.G. Ghielmetti, E.S. Clarflin, T.E. Moore, M.R. Collier, H.U. Frey, and S.B. Mende, Localized ion outflow in response to solar wind pressure pulse, *J. Geophys. Res.*, *107*(A8), SMP 26, doi: 10.1029/2001JA000297, 2002.

Ghielmetti, A.G., E.G. Shelley, S.A. Fuselier, P. Wurz, P. Bochsler, F.A. Herrero, M.F. Smith, and T.M. Stephen, Mass spectrograph for imaging low-energy neutral atoms, *Optical Eng.*, *33*, 362, 1994.

Giles, B.L., Inner magnetosphere circulation of thermal ions inferred from observed pitch angle distributions, Ph.D Thesis, University of Alabama in Huntsville, Huntsville, 1993.

Heelis, R.A., G.J. Bailey, R. Sellek, R.J. Moffet, B. Jenkins, Field-aligned drifts in subauroral ion drift events, *J. Geophys. Res.*, *98*, 21493, 1993.

Horwitz J.L. and T.E. Moore, Four contemporary issues concerning ionospheric plasma flow in the magnetosphere, *Space Sci. Rev.*, *80*, 49, 1997.

Khan, H., and S.W.H. Cowley, Observations of the response time of high latitude ionospheric convection to variations in the interplanetary magnetic field using EISCAT and IMP-8 data, *Ann. Geophysicae*, *17*, 1306, 1999.

Kokubun, S., T. Yamamoto, M.H. Acuña, K. Hayashi, K. Shirokawa, and H. Kawano, The Geotail magnetic field experiment, *J. Geomagn. Geoelectr.*, *46*, 7, 1994.

Lennartsson, O.W., A scenario for solar wind penetration of Earth's magnetic tail based on ion composition data from ISEE 1 spacecraft, *J. Geophys. Res.*, *97*, 19222, 1992.

Lockwood, M., J.H. Waite, Jr., T.E. Moore, J.F.E. Johnson, and C.R. Chappell, A new source of supathermal O^+ ions near the dayside polar cap boundary, *J. Geophys. Res.*, *90*, 4099, 1985.

Lundin, R., L.R. Lyons, and N. Pissarenko, Observations of the ring current composition at L=4, *Geophys. Res. Lett.*, *7*, 425, 1980.

Moore, T.E., C.R. Chappel, M. Lockwood, and J.H. Waite, Jr., Supathermal ion signatures of auroral acceleration processes, *J. Geophys. Res.*, *90*, 1611, 1985.

Moore, T.E., M. Lockwood, M.O. Chandler, J.H. Waite, Jr., C.R. Chappell, A. Persoon, and M. Sugiura, Upwelling O+ ion source characteristics, *J. Geophys. Res.*, *91*, 7019, 1986.

Moore, T.E., W.K. Peterson, C.T. Russell, M.O. Chandler, M.R. Collier, H.L. Collin, P.D. Craven, R. Fitzenreiter, B.L. Giles, C.J. Pollock, Ionospheric mass ejection in response to CME, *Geophys. Res. Lett.*, *26*, 2339, 1999.

Moore, T.E., et al., The low energy neutral atom imager for IMAGE, *Space Sci. Rev.*, *91*, 155, 2000.

Moore, T.E., M.R. Collier, J.L. Burch, D.J. Chornay, S.A. Fuselier, A.G. Ghielmetti, B.L. Giles, D.C. Hamilton, F.A. Herrero, J.W. Keller, K.W. Ogilvie, B.L. Peko, J.M. Quinn, T.M. Stephen, G.R. Wilson, and P. Wurz, Low energy neutral atoms in the magnetosphere, *Geophys. Res. Lett.*, *28*, 1143, 2001.

Øieroest, M., M. Yamauchi, L. Liska, and B. Hultqvist, Energetic ion outflow from the dayside ionosphere: Categorization, classification, and statistical study, *J. Geophys. Res.*, *104*, 24915, 1999.

Pollock., C.J., M.O. Chandler, T.E. Moore, J.H. Waite, Jr., C.R. Chappell, and D.A Gurnett, A survey of upwelling ion event characteristics, *J. Geophys. Res.*, *95*, 18969, 1990.

Sharp, R.D., D.L. Carr, W.K. Peterson, and E.G. Shelley, Ion streams in the magnetotail, *J. Geophys. Res.*, *86*, 4639, 1981.

Shelley, E.G., R.G. Johnson, and R.D. Sharp, Satellite observations of energetic heavy ions during a geomagnetic storm, *J. Geophys. Res.*, *77*, 6104, 1972.

Shelley, E.G., R.D. Sharp, and R.G. Johnson, Satellite observations of an ionospheric acceleration mechanism, *Geophys. Res. Lett.*, *3*, 654, 1976.

Shelley, E.G., Circulation of energetic ions of terrestrial origin in the magnetosphere, *Adv. Space Sci.*, *5*, 401, 1985.

Waite, J.H. Jr, T. Nagai, J.F.E. Johnson, C.R. Chappell, J.L. Burch, T.L. Killeen, P.B. Hays, G.R. Carignan, W.K. Peterson, and E.G. Shelley, Escape of suprathermal O+ ions in the polar cap, *J. Geophys. Res.*, *90*, 1619, 1985.

Wurz, P., M.R. Aellig, P. Bochsler, A.G. Ghielmetti, E.G. Shelley, S.A Fuselier, F.A. Herrero, M.F. Smith, and T.M. Stephen, Neutral atom imaging mass spectrograph, *Optical Eng.*, *34*, 2365, 1995.

Yau, A.W., B.A. Whalen, A.G. McNamara, P.J. Kellogg, and W. Bernstein, Particle and wave observations of low-latitude ionospheric ion acceleration events, *J. Geophys. Res.*, *88*, 341, 1983.

Yau, A.W., E.G. Shelley, W.K. Peterson, and L. Lenchyshyn, Energetic auroral and polar ion outflow at DE 1 altitudes: Magnetic, composition, magnetic activity dependence, and long term variation, *J. Geophys. Res.*, *90*, 8417, 1985.

Yau, A.W., and M Lockwood, Observations of ionospheric outflow, in *Modelling Magnetospheric Plasma, Geophys. Monogr. Ser.*, vol. 44, edited by T.E. Moore and J.H. Waite Jr., pp. 229, AGU, Washington, D.C., 1988.
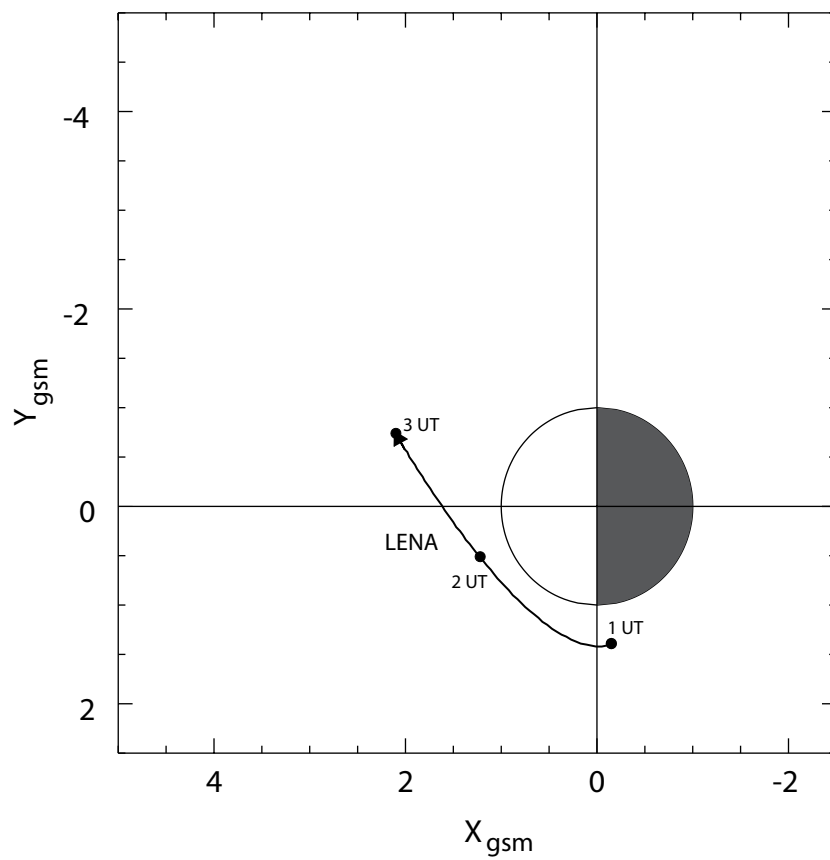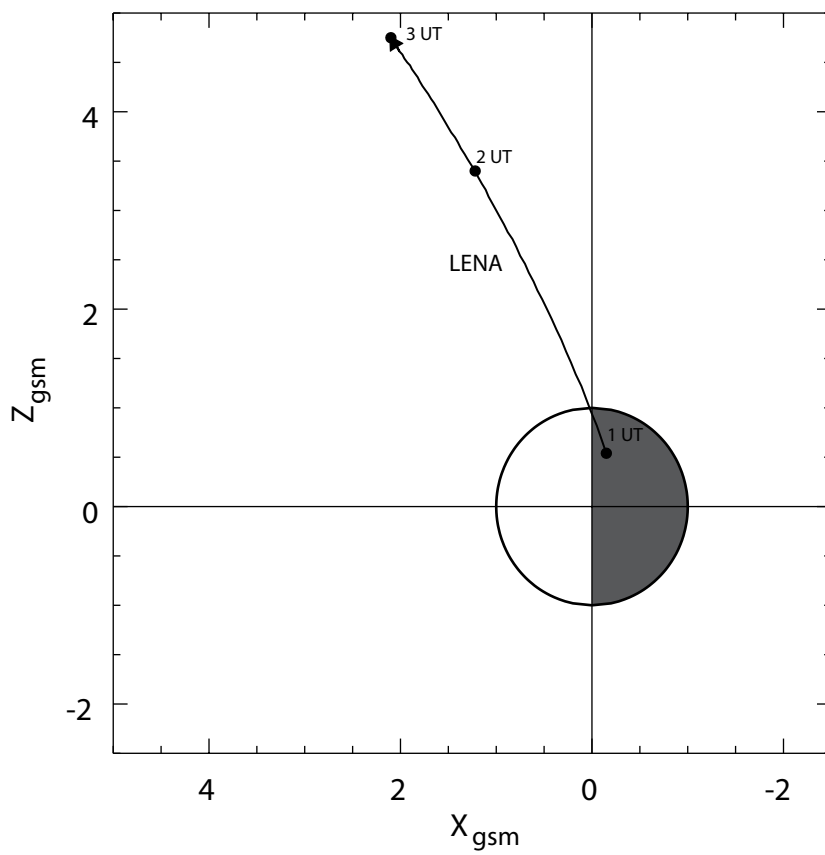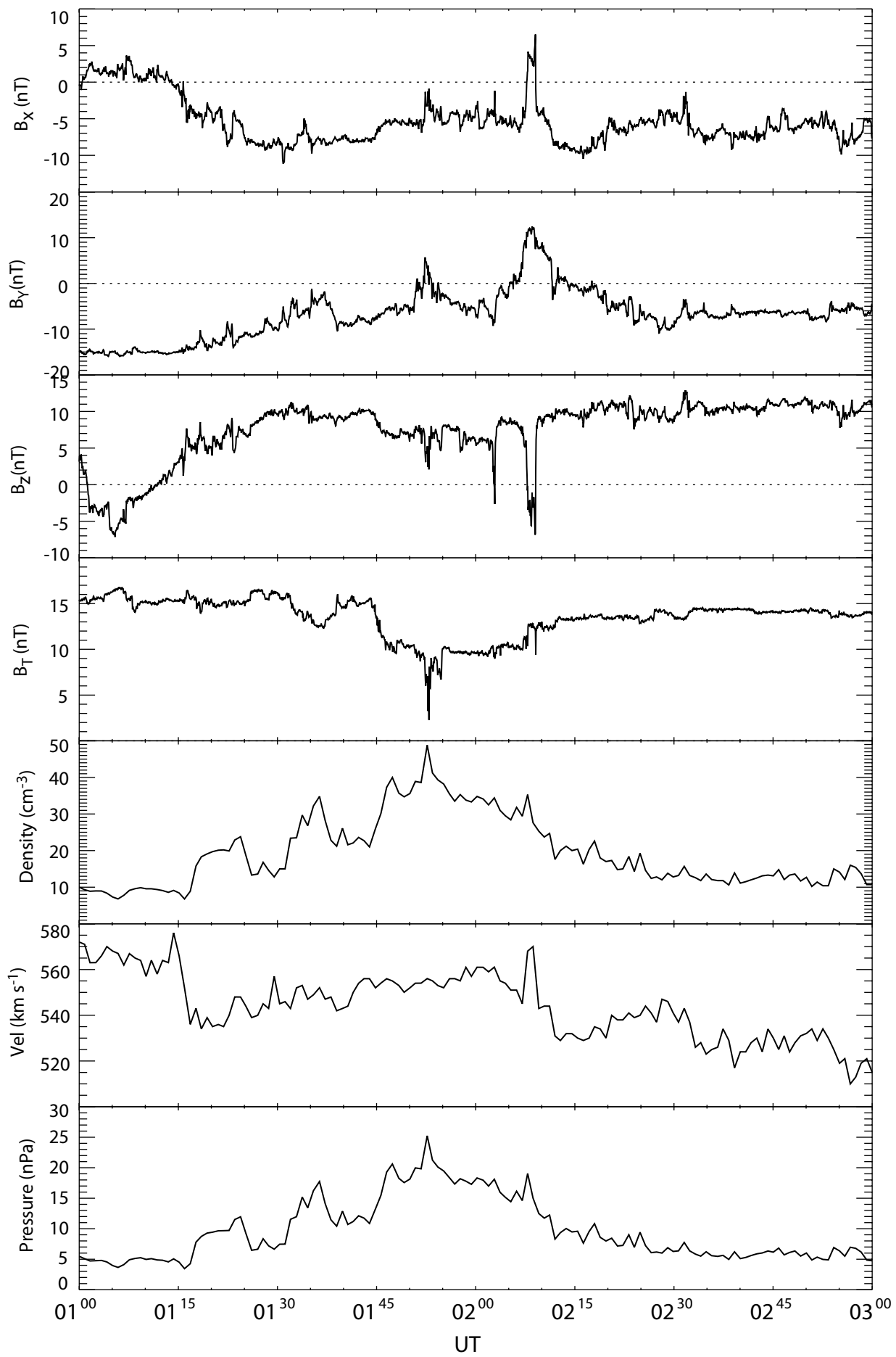
X,R$_E$ 18.0900	18.6110	19.0778
Y,R$_E$ 1.03162	1.85579	2.66040
Z,R$_E$ -2.57730	-2.49716	-2.48901

IMAGE/LENA Singles & Coincidences Event
Start Time: 2000/06/24 (176) 01:00:00
Stop Time: 2000/06/24 (176) 03:00:00

sun
ram
B

no data
no cnts

Starts — Earth Cntrd Azi — log Cnt Rate [Hz]

Stops — Earth Cntrd Azi — log Cnt Rate [Hz]

Event 10eV–300eV — Earth Cntrd Azi — log atoms/cm2/s

UT	01:00	01:20	01:40	02:00	02:20	02:40	03:00	hh:mm
Lshell	1.00	6.00	30.00	143.00	292.00	172.00	105.00	
RE	1.50	2.25	2.99	3.65	4.25	4.78	5.26	Re
MLT	17.73	15.26	13.69	12.72	12.09	11.65	11.33	hrs
MLat	21.49	39.89	42.78	41.76	39.86	37.89	36.08	degs
InvLat	0.00	65.91	79.48	85.20	86.65	85.63	84.40	degs

Solar wind pressure:
0020-0330 UT

LENA Hydrogen cnts:
0120-0230 UT

Solar wind pressure:
0020-0330 UT

LENA Oxygen cnts:
0120-0230 UT

Solar wind pressure:
0020-0330 UT

LENA Oxygen cnts:
0120-0230 UT

Pressure (nPa)
Solid Line

LENA Hydrogen cnts
Dashed Line

Solar wind pressure:
0020-0330 UT

LENA Hydrogen cnts:
0120-0230 UT

25

20

15

10

5

80

60

40

20

0

00³⁰   01⁰⁰   01³⁰   02⁰⁰   02³⁰   03⁰⁰

Time

1.0

0.5

0.0

-0.5

-1.0

Cross Correlation Coefficient

-60   -40   -20   0   20   40   60

Time lags (mins)

80

60

40

20

0

-20

Hydrogen Counts

5   10   15   20   25

Pressure (nPa)